Chapter 20

The Martini Coarse-Grained Force Field

Xavier Periole and Siewert-Jan Marrink

Abstract

The Martini force field is a coarse-grained force field suited for molecular dynamics simulations of biomolecular systems. The force field has been parameterized in a systematic way, based on the reproduction of partitioning free energies between polar and apolar phases of a large number of chemical compounds. In this chapter the methodology underlying the force field is presented together with details of its parameterization and limitations. Then currently available topologies are described with a short overview of the key elements of their parameterization. These include the new polarizable Martini water model. A set of three selected ongoing studies using the Martini force field is presented. Finally the latest lines of development are discussed.

Key words: Coarse-grained models, Martini force field, Molecular dynamics simulations, Biomolecular systems

1. Introduction

The use of coarse-grained (CG) models in a variety of simulation techniques has proven to be a valuable tool to probe the time and length scales of systems beyond what is feasible with traditional all-atom (AA) models. Applications to lipid systems in particular, pioneered by Smit et al. (1), have become widely used. A large diversity of coarse-graining approaches is available; they range from qualitative, solvent-free models, via more realistic models with explicit water, to models including chemical specificity (for recent reviews see refs. 2–4). Models within this latter category are typically parameterized based on comparison to atomistic simulations, using iterative Boltzmann schemes (5–7) or force matching (8) approaches. Our own model (9, 10), coined the Martini force field, has also been developed in close connection with atomistic models; however, the philosophy of our coarse-graining approach is different. Instead of focusing on an accurate reproduction of structural details at a particular state point for a specific system, we aim for

Luca Monticelli and Emppu Salonen (eds.), *Biomolecular Simulations: Methods and Protocols*, Methods in Molecular Biology, vol. 924, DOI 10.1007/978-1-62703-017-5_20,

a broader range of applications without the need to reparameterize the model each time. We do so by extensive calibration of the chemical building blocks of the CG force field against thermodynamic data, in particular oil/water partitioning coefficients. This is similar in spirit to the recent development of the GROMOS force field (11). Processes such as lipid self-assembly, peptide membrane binding, and protein–protein recognition depend critically on the degree to which the constituents partition between polar and nonpolar environments. The use of a consistent strategy for the development of compatible CG and atomic-level force fields is of additional importance for its intended use in multiscale applications (12). The overall aim of our coarse-graining approach is to provide a simple model that is computationally fast and easy to use, yet flexible enough to be applicable to a large range of biomolecular systems. Detailed tutorials have been made available for people to be able to play around with simple systems and thereby get their hands on the different aspects of coarse-graining and running different types of systems. These tutorials are downloadable free of charge from the Martini Web site: http://cgmartini.nl.

Currently, the Martini force field provides parameters for a variety of biomolecules, including many different lipids, cholesterol, amino acids, sugars, DNA, fullerene, collagen, dendrimers, and more. A protocol for simulating peptides and proteins is also available. Extensive comparison of the performance of the Martini model with respect to a variety of experimental properties has revealed that the model performs generally quite well ("semi-quantitatively") for a broad range of systems and state points. Properties accurately reproduced include structural (e.g., liquid densities (9), area/lipid for many different lipid types (9), accessible lipid conformations (13), the tilt angle of membrane spanning helices (14), or helix-helix packing motifs (15, 16), elastic (e.g., bilayer bending modulus (9), rupture tension (10)), dynamic (e.g., diffusion rates of lipids (9, 10), peptides (17) and proteins (18), water transmembrane (TM) permeation rate (9), time scales for lipid aggregation (9)), and thermodynamic (e.g., bilayer phase transition temperatures (19, 20), propensity for interfacial versus TM peptide orientation (14), lipid desorption free energy (10), membrane domain formation (21, 22)) data.

The remainder of this chapter is organized as follows. A detailed description of the CG methodology is presented in the next section, discussing both its abilities and its limitations. Subsequently, a nonexhaustive list of currently available topologies is given and finally examples of three applications are presented, namely, the molecular face of lipid rafts, the gating of a membrane-embedded mechanosensitive channel, and evidence for binding sites of cardiolipins mediating mitochondrial supercomplex formation. A short look at the future prospects of the Martini force field concludes this chapter.

2. General Methodology

2.1. The Looks of Martini

The name: The name "Martini" of the force field was coined in 2007 with the release of version 2.0 (10). Martini is the nickname of the city of Groningen in the Netherlands where the force field was developed and where its development continues to date. A famous landmark in the city is the 100 m high Martini tower. The name also reflects the universality of the cocktail with the same name; how a few simple ingredients (chemical building blocks) can be endlessly varied to create a complex palette of taste.

The mapping: The Martini model is based on a four-to-one mapping (10), i.e., on average four heavy atoms are represented by a single interaction center, with an exception for ring-like molecules. To map the geometric specificity of small ring-like fragments or molecules (e.g., benzene, cholesterol, and several of the amino acids), the general four-to-one mapping rule is insufficient. Ring-like molecules are therefore mapped with higher resolution (up to two-to-one). The model considers four main types of interaction sites: polar (P), nonpolar (N), apolar (C), and charged (Q). Within a main type, subtypes are distinguished either by a letter denoting the hydrogen-bonding capabilities (d = donor, a = acceptor, da = both, 0 = none) or by a number indicating the degree of polarity (from 1 = low polarity to 5 = high polarity). The mapping of representative biomolecules is shown in Fig. 1. For reasons of computational efficiency the mass of the CG beads is set to 72 amu (corresponding to four water molecules) for all beads, except for beads in ring structures, for which the mass is set to 45 amu.

Nonbonded interaction potentials: All particle pairs i and j at distance r_{ij} interact via a Lennard-Jones (LJ) potential:

$$V_{\mathrm{LJ}} = 4\varepsilon_{ij}[(\sigma_{ij})^{12} - (\sigma/r_{ij})^{6}] \quad (1)$$

The strength of the interaction, determined by the value of the well-depth ε_{ij}, depends on the interacting particle types. The value of ε ranges from $\varepsilon_{ij} = 5.6$ kJ/mol for interactions between strongly polar groups to $\varepsilon_{ij} = 2.0$ kJ/mol for interactions between polar and apolar groups mimicking the hydrophobic effect. The effective size of the particles is governed by the LJ parameter $\sigma = 0.47$ nm for all normal particle types. For the special class of particles used for ring-like molecules, slightly reduced parameters are defined to model ring-ring interactions; $\sigma = 0.43$ nm, and ε_{ij} is scaled to 75% of the standard value. The full interaction matrix can be found in the original publication (10). In addition to the LJ interaction, charged groups (type Q) bearing a charge q interact via a Coulombic energy function with a relative dielectric constant $\varepsilon_{\mathrm{rel}} = 15$ for explicit screening:

$$V_{\mathrm{el}} = q_i q_j / 4\pi\varepsilon_0 \varepsilon_{\mathrm{rel}} r_{ij} \quad (2)$$

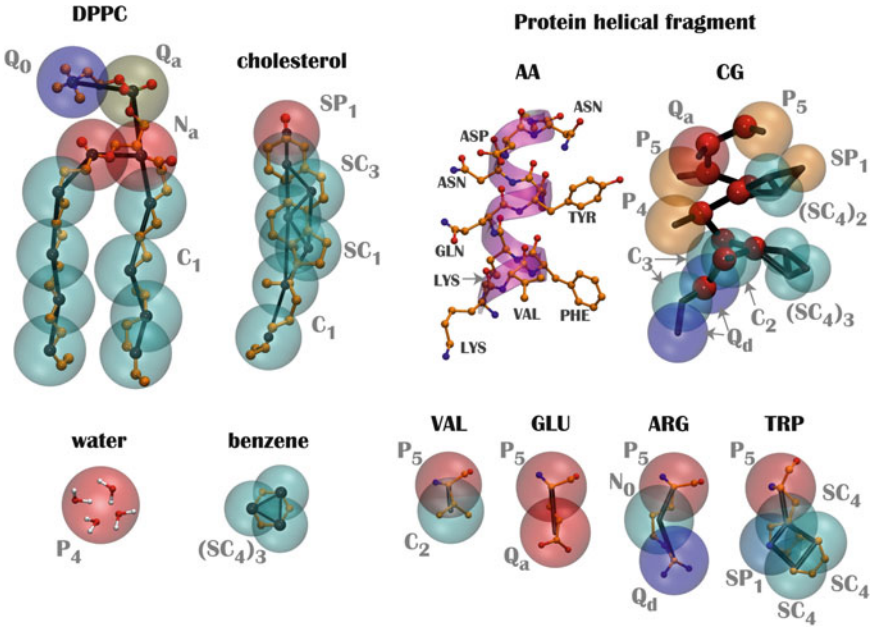

Fig. 1. The looks of Martini. Mapping between the chemical structure at the atomistic level (AA) with the coarse-grained (CG) Martini model for DPPC, cholesterol, water, benzene, a protein helical fragment, and a few amino acids (valine, glutamic acid, arginine, and tryptophan). The CG beads are shown as transparent vdW spheres. For clarity, in the case of the protein helical fragment the AA and CG representations are shown side-by-side and the CG backbone beads are represented by small spheres. Hydrogens are only shown for the atomistic water.

Note that the nonbonded potential energy functions are used in their shifted form. The nonbonded interactions are cut off at a distance $r_{\text{cut}} = 1.2$ nm. The LJ potential is shifted from $r_{\text{shift}} = 0.9$ nm to r_{cut}. The electrostatic potential is shifted from $r_{\text{shift}} = 0.0$ nm to r_{cut}. Shifting of the electrostatic potential in this manner mimics the effect of a distance-dependent screening.

Bonded interaction potentials: Bonded interactions are described by the following set of potential energy functions:

$$V_{\text{b}} = 1/2 K_{\text{b}} (d_{ij} - d_{\text{b}})^2, \tag{3}$$

$$V_{\text{a}} = 1/2 K_{\text{a}} [\cos(\varphi_{ijk}) - \cos(\varphi_{\text{a}})]^2, \tag{4}$$

$$V_{\text{d}} = K_{\text{d}} [1 + \cos(\theta_{ijkl} - \theta_{\text{d}})], \tag{5}$$

$$V_{\text{id}} = K_{\text{id}} (\theta_{ijkl} - \theta_{\text{id}})^2, \tag{6}$$

acting between bonded sites i, j, k, l with equilibrium distance d_{b}, angle φ_{a}, and dihedral angles θ_{d} and θ_{id}. The force constants K are generally weak, inducing flexibility of the molecule at the CG level resulting from the collective motions at the fine-grained level. The bonded potential V_{b} is used for chemically bonded sites, and the

angle potential V_a to represent chain stiffness. Proper dihedrals V_d are presently only used to impose secondary structure of the peptide backbone, and the improper dihedral angle potential V_{id} is used to prevent out-of-plane distortions of planar groups. LJ interactions between nearest neighbors are excluded.

Implementation: The functional form of the CG force field was originally developed for convenient use with the GROMACS simulation software (23). Example input files for many systems can be downloaded from http://cgmartini.nl. The current version of the Martini force field is denoted as version 2.0 (lipids only) or 2.1 (including proteins). The general form of the potential energy functions has allowed other groups to implement our CG model (with small modifications) also into other major simulation packages such as NAMD (24), GROMOS (13) and Desmond (25). Note that the groups of Schulten (26, 27) and Sansom (28, 29) have developed CG protein force fields compatible with the Martini lipid force field, but different from the Martini protein force field.

2.2. Parameterization of Nonbonded Interactions

In order to parameterize the nonbonded interactions of the CG model, a systematic comparison to experimental thermodynamic data has been performed. Specifically, the free energy of hydration, the free energy of vaporization, and the partitioning free energies between water and a number of organic phases were calculated for each of the 18 different CG particle types. Concerning the free energies of hydration and vaporization, the CG model reproduces the correct trend (10). The actual values are systematically too high, however, implying that the CG condensed phase is not as stable with respect to the vapor phase as it should be. The same is true with respect to the solid phase. This is a known consequence of using a LJ 12-6 interaction potential, which has a limited fluid range. Switching to a different nonbonded interaction potential could, in principle, improve the relative stability of the fluid phase (see Subheading 5). As long as its applications are aimed at studying the condensed phase and not at reproducing gas/fluid or solid/fluid coexistence regions, the most important thermodynamic property is the partitioning free energy. Importantly, the water/oil partitioning behavior of a wide variety of compounds can be accurately reproduced with the current parameterization of the Martini model. Table 1 shows results obtained for the partitioning between water and a range of organic phases of increasing polarity (hexadecane, chloroform, and octanol) for a selection of the 18 CG particle types. The free energy of partitioning between organic and aqueous phases, $\Delta G_{oil/aq}$, was obtained from the equilibrium densities ρ of CG particles in both phases:

$$\Delta G_{oil/aq} = kT \ln (\rho_{oil}/\rho_{aq}) \quad (7)$$

Table 1
Oil (Hex), chloroform (CLF), and octanol (OCO)/water partitioning free energies for a selection of the 18 CG particle types, compared to experimental values of the corresponding chemical building blocks

		Hex/water		CLF/water		OCO/water	
Building block	**Type**	**CG**	**Exp**	**CG**	**Exp**	**CG**	**Exp**
Acetamide	P_5	−28	−27	−18	−20	−10	−8
Water	P_4	−23	−25	−14	–	−9	−8
Propanol	P_1	−11	−10	−2	−2	−1	0
Propylamine	N_d	−7	−6	0	1	3	3
Methylformate	N_a	−7	−6	0	4	3	0
Methoxyethane	N_0	−2	1	6	–	5	3
Butadiene	C_4	9	11	13	–	9	11
Chloropropane	C_3	13	12	13	–	14	12
Butane	C_1	18	18	18	–	17	16

The experimental data are compiled from various sources (see ref. 10), the simulation data are obtained using Eq. 7. All values are expressed in kJ/mol and obtained at T = 300 K

The equilibrium densities can be obtained directly from a long MD simulation of the two-phase system in which small amounts (around 0.01 mole fraction proved sufficient to be in the limit of infinite dilution) of the target substance are dissolved. With the CG model, simulations can easily be extended into the multimicrosecond range, enough to obtain statistically reliable results to within 1 kJ/mol for most particle types. As can be judged from Table 1, comparison to experimental data for small molecules containing four heavy atoms (the basic mapping of the CG model) reveals a close agreement to within 2 kT for almost all compounds and phases; indeed, agreement is within 1 kT for many of them. Expecting more accuracy of a CG model might be unrealistic. Note that the multiple nonbonded interaction levels allow for discrimination between chemically similar building blocks, such as saturated versus unsaturated alkanes or propanol versus butanol (which would be modeled as Nda) or ethanol (P2). A more extensive table including all particle types and many more building blocks can be found in the original publication (10).

The thermodynamic integration (TI) approach is also routinely used to determine solute partitioning free energies. It has a few advantages over the equilibrated two-phase technique: (1) it avoids uncertainties due to finite concentration effect since it truly reflects infinite dilution, (2) it solves the sampling issue observed in cases

where the solute favors one phase much more than the other. The use of TI coupled with a thermodynamic cycle for the calculation of solvation free energy is well documented in the literature. One may consult the article from Villa and Mark for a detailed description (30). Technical aspects of the calculation using the Gromacs package are described in a tutorial available on the Martini Web site. A comparison of solvation free energies obtained with TI compared to the direct approach is given in (31).

2.3. Parameterization of Bonded Interactions

To parameterize the bonded interactions, we use structural data that are either directly derived from the underlying atomistic structure (such as bond lengths of rigid structures) or obtained from comparison to fine-grained simulations. In the latter procedure, the fine-grained simulations are first converted into a "mapped" CG (MCG) simulation by identifying the center-of-mass of the corresponding atoms as the MCG bead. Second, the distribution functions are calculated for the mapped simulation and compared to those obtained from a true CG simulation. Subsequently the CG parameters are systematically changed until satisfactory overlap of the distribution functions is obtained. Using this procedure, simulations of bulk alkanes have been used to determine the optimal values of the "standard" equilibrium bond distance of 0.47 nm and force constant of $K_b = 1{,}250$ kJ/mol/nm^2, and equilibrium angle of 180° with force constant of $K_a = 25$ kJ/mol. Likewise, standard bonded parameters have been derived for unsaturated alkanes (10), and the phospholipid headgroup (9).

Although it is advised to try sticking to the use of COM of atom groups in the mapping, in cases of complex molecules it might be more convenient to use specific atoms instead. This would be fine and might for instance allow a better representation of the mechanistic of the molecule e.g., to represent the relative orientation of two bound planes (aromatics) it would be important to realistically incorporate the rotation around the bond into the model. This might be easier using specific sites in the atomistic model. In extreme cases it might even be necessary to use a "double bead" representation in which one bead caries the bonded terms while the other one carries the nonbonded terms. In this approach it is important to choose the link between the two beads adequately (virtual sites may be used). This solution should not be a standard.

2.4. Limitations of the Model

The potential range of applications of the CG model is very broad. There are, however, certain important limitations that should be kept in mind.

Limited stability of fluid phase: First of all, the model has been parameterized for the fluid phase. Properties of solids, such as crystal packing, are not expected to be accurate. Both the gas and the solid phase appear too stable with respect to the fluid phase.

This is a known consequence of the use of the LJ 12-6 potential for the nonbonded interactions. The thermodynamic behavior of solid–fluid and gas–fluid interfaces should therefore be interpreted with care, at least at the quantitative level. In applications where such interfaces are formed (especially the water–vapor interface in, e.g., rupture of lipid monolayers) these limitations have to be kept in mind. In biomolecular simulations, a related problem is the potential freezing of the Martini water model. The LJ parameters for water ($\varepsilon = 5.0$ kJ/mol, $\sigma = 0.47$ nm) bring it into the solid state region of the LJ phase diagram, although the use of a shift potential reduces the long-range attractive part and the CG water is more fluid compared to the standard LJ particle. We have previously determined the freezing temperature of the CG water as 290 ± 5 K (9, 10, 32). While this is admittedly higher than it should be, in most applications freezing is not observed as long as no nucleation site is formed. Apart from simulations performed at lower temperatures, rapid freezing is a potential problem in systems where a nucleation site is already present (a solid surface, but also an ordered bilayer surface may act as one) or when periodicity enhances the long-range ordering (e.g., for small volumes of water). In those cases in which the freezing poses a problem, a simple pragmatic solution has been presented in the form of antifreeze particles (10). This works in some cases, but has apparently given problems in combination with solid supports (33). Freezing might also be more easily observed with Martini implementations in other packages, notably with Gromos which uses an extended LJ interaction (13).

Entropy-enthalpy compensation: Furthermore, the parameterization is based on free energies. The inherent entropy loss on coarse graining is necessarily compensated for by a reduced enthalpy term (13). The enthalpy/entropy balance of many processes may therefore be biased when modeled at the CG level and affect its temperature dependence, although not necessarily weakening it. For instance, the temperature-dependent hydration free energy for linear alkanes was found to be more pronounced in the CG representation compared to an AA representation (13). As is true for any force field, applications outside the temperature range used for parameterization (~270–330 K) have to be considered with care. Although absolute entropies are clearly underestimated due to the loss of atomistic degrees of freedom, entropy differences can still be accurate. As an example, for the dimerization of WALP23 in DOPC, a direct comparison of enthalpies and entropies obtained from experiment and simulation is possible: Yano and Matsuzaki (34) measured values of $\Delta H = -31$ kJ/mol and $\Delta TS = +19$ kJ/mol, which can be compared to the respective values of −30 kJ/mol and +15 kJ/mol obtained by Ash and coworkers (35) using the Martini force field. Thus, not only is the dimerization free energy difference ΔG obtained with the Martini model (−15 kJ/mol) in good agreement with experiment (−13 kJ/mol), but also the enthalpic and entropic contributions to it.

Implicit screening: Another difficulty encountered in our CG model, and perhaps in most coarse-graining approaches, is the correct modeling of the partitioning of polar and charged compounds into a low dielectric medium. Because of the implicit screening, the interaction strength of polar substances is underestimated in nonpolarizable solvents. Applications involving the formation of polar/charged complexes in a nonpolar environment are especially prone to be affected. The inability to form a TM water pore upon dragging a lipid across the membrane is an example (10). The recent development of a Martini water model that includes orientational polarization by the means of a dipole represented by two drude charges attached to each water bead (see below for a detailed description) allows to correct for some of these effects (31). Apart from the implicit screening in the CG model, the neglect of long-range electrostatic forces poses a further limitation. Pairwise interactions beyond 1.2 nm (between two and three CG beads away) are not taken into account. In principle long-range electrostatic interactions could be added to the CG model, in ways similar to those used in atomistic simulations. One has to realize that a modification of the electrostatic interaction scheme might affect other system properties.

Effective time scale: The CG dynamics is faster than the AA dynamics because the CG interactions are much smoother compared to atomistic interactions. The effective friction caused by the fine-grained degrees of freedom is missing. Based on comparison of diffusion constants for a range of systems (including simple solvents and lipids) in the CG model versus experimental data, the effective time sampled using CG interactions is three- to eightfold larger. When interpreting the simulation results with the CG model, a standard conversion factor of 4 is used, which is the effective speed-up factor in the diffusion dynamics of CG water compared to real water. The same order of acceleration of the overall dynamics is also observed for a number of other processes, including the permeation rate of water across a membrane (9), the sampling of the local configurational space of a lipid (13), the aggregation rate of lipids into bilayers (9) or vesicles (23), and the self-diffusion of lipids (9, 10), transmembrane peptides (17), and proteins (18). However, the speed-up factor might be quite different in other systems or for other processes. Particularly for protein systems, no extensive testing of the actual speed-up due to the CG dynamics has been performed, although protein translational and rotational diffusion was found to be in good agreement with experimental data in simulations of CG rhodopsin (18). In general, the time scale of the simulations has to be interpreted with care.

Time step: Martini has been parameterized using time steps in the range of 20–40 fs. Whether you can use 40 fs or have to settle for a somewhat smaller time step depends on your system, and on your

attitude toward coarse-grained modeling, as explained below. First, the Martini force field is not an atomistically detailed force field. Many assumptions underlie the model, the major one being the neglect of some of the atomistic degrees of freedom. As a result, the interactions between particles are effective ones and the energy landscape is highly simplified. This simplified energy landscape allows for a greatly increased sampling speed at the cost of a loss of detail. This makes CG models in general so powerful. The emphasis, therefore, should not be to sample the energy landscape as accurately as possible, but rather, as effectively as possible. This is in contrast to traditional all-atom models, for which the energy landscape is more realistic and an accurate integration scheme is more important. In practice, the inherent "fuzziness" of the Martini model makes the presence of small energy sinks or sources a less critical problem than in accurate atomistic simulations. Second and most importantly, structural properties are rather very robust with respect to time step; for a time step up to 40 fs, there are no noticeable effects on structural properties of the systems investigated. Moreover, thermodynamic properties such as the free energy of solvation also appear insensitive to the size of the time step. Thus, if the goal is to generate representative ensembles quickly, large time steps seem acceptable. Whereas one can debate the first argument (i.e., the "idealist" versus "pragmatic" view of the power of CG simulations), the second argument (i.e., the insensitivity of both structural and thermodynamic properties to the magnitude of the time step) implies that a reduction of the time step to 10 fs or below, as recently suggested (36), is a waste of computer time (32). Nevertheless, time steps of 40 fs and beyond may be pushing the limits too far for certain systems. We therefore recommend a time step of 20–30 fs, in combination with an enlarged neighborlist cutoff (to 1.4 nm) to be on the safe side. Of course, one should always check whether or not results are biased by the choices made. Given that the largest simplifications are made at the level of the interaction potentials, this can best be done by comparing to results obtained using more detailed models.

Fixed secondary structure: Finally, in applications of peptides and proteins one has to be aware that secondary structure (SS) transformations are not modeled in the current parameterization (see Subheading 3). The secondary structure is essentially fixed by the use of a dihedral potential energy function. The backbone bead type is also function of the SS to take into account the fact that when involved in interactions stabilizing a given SS element the backbone is less prompted to engage in other interactions. The backbone interaction strength is therefore decreased when involved in a SS element. This approach allows discrimination between various secondary structure elements but prevents realistic transitions between them. Processes in which folding and unfolding are playing a substantial role are therefore not suitable for modeling

with our current CG force field. Movements of secondary structure elements with respect to each other are possible, however, and were shown to be quite realistic in a recent application of the gating of a membrane-embedded mechanosensitive channel (see Subheading 4).

3. Available Topologies

The transferability that the Martini model has been conceived on has been used by our group but also by other groups to make topologies for generic building blocks for several molecule types as lipids, proteins, sugars, but also for more specific ones such as fullerene, DNA, collagen, and polymers. Of special interest is also the recently developed topology for a polarizable water model. The topologies are available on the Martini Web site: http://cgmartini.nl, and discussed in some detail below. A general recipe for construction of your own model is also given.

3.1. Basic Topologies for Lipids, Proteins, Sugars

Lipids: The Martini force field has been originally developed with a strong orientation toward lipid systems. The lipid models have been thoroughly tested on many types of systems covering not only the bilayer state but also micellar, monolayer, hexagonal, and cubic phases. An example topology for a dipalmitoyl-phosphatidylcholine (DPPC) molecule is shown in Fig. 1a. The hydrophobic tails consist of C1 type particles, the glycerol moiety of Na particles of intermediate polarity, and the head group of a negatively charged Qa particle for the phosphate group, and a positively charged Q0 particle for the choline group. Double bonds in the tail can be effectively modeled using slightly less hydrophobic beads (C2, C3) together with a change of the angle potential (Eq. 4) that governs the stiffness and orientation of the lipid tails. Likewise, changes in the lipid head group particle types allow one to discriminate between the most important lipid classes. Currently available topologies include PC (phosphatidylcholine), PE (phosphatidylethanolamine), PG (phosphatidylglycerol), and PS (phosphatidylserine), with all common tails such as hexanoyl, lauroyl, palmitoyl, oleoyl, stearoyl, linoleyl, and arachidonoyl tails. The properties that are reproduced with these models include structural (area per lipid and bilayer thickness), elastic (bending rigidity and area compressibility), thermodynamic (phase transition temperature and line tension) and dynamical (lipid diffusion and water permeation rate) data. In addition to two-tail lipids, the topologies of a variety of single-tail lipids are available, as well as for sphingolipid (SM). However, parameterization of the latter has proven problematic due to lack of clear experimental data and consistent atomistic models for SM bilayers. Furthermore, lipid topologies have been parameterized for specific lipids such

as cholesterol (37, 38), cardiolipins (39), triglycerides (40), and bolalipids (41).

Proteins: To select particle types for the amino acids, systematic comparison to experimental partitioning free energies between polar and apolar media was also used in line with the general Martini philosophy (see Subheading 2). Table 2 shows the resulting assignment of the amino acid side chains and the associated partitioning free energies. Where available, the experimental values are reproduced to within 2 kT, a level of accuracy that is difficult to obtain even with atomistic models. Most amino acids are mapped onto single standard particle types, similarly to the recent work of other groups (26, 29). The positively charged amino acids are modeled by a combination of a Q-type and an N- or C-type particle. The bulkier ring-based side chains are modeled by three or four beads of the special class of ring particles. The Gly and Ala residues are only represented by the backbone particle. Figure 1 shows the mapping of a few of them. To compensate for the lack of directionality in the backbone interactions (H-bonds) the type of the particle used for the backbone bead is made a function of its secondary structure; when free in solution or in a coil or bend, the backbone has a strong polar character (P type), while as part of a helix or beta strand the interbackbone hydrogen bonds reduce the polar character significantly (N type). The final bead type of each amino acid was refined to match data obtained from atomistic simulations: (1) PMF of side chain analogues when crossing a DOPC–water interface, (2) amino acid association constants, (3) partitioning and orientation of pentapeptides at the water–cyclohexane interface, (4) tilt, orientation and interaction of helical transmembrane peptides (14).

For the bonded interactions, distributions were derived directly from the protein databank, using the proper AA to CG mapping (14). These distributions reflect all possible configurations for a large number of different systems under a variety of conditions. Keeping the aim of our CG model in mind, namely, to be able to simulate many biomolecules with a single set of parameters, this is the least biased information. Using this procedure, bonded parameters were derived for the backbone (BB) potentials, namely, the BB-BB bonded potential, the BB-BB-BB angle potential, and the BB-BB-BB-BB dihedral potential. Furthermore, for each amino acid, side chain (SC) distributions were obtained for the BB-SC bonded potential, the BB-BB-SC angle potential, and for the intra-SC potentials for amino acids containing more than one CG particle. The complete set of bonded and nonbonded parameters for proteins can be found elsewhere together with more details of the parameterization (14). In the current version of Martini the BB-BB-BB angle potential, and the BB-BB-BB-BB dihedral potential are used to enforce the secondary structure (SS) of the backbone, which is therefore an input parameter in our CG model. Different

Table 2
Free energy based mapping of select amino acid side chain analogues

			Oil/water	
Side chain	**Particle type**	**Mapping[a]**	**CG**	**Exp**
LEU/ILE	C1		22	22/22
VAL/PRO	C2		20	17/–
MET/CYS	C5		9	10/5
SER/THR	P1		−11	−14/−11
ASN	P5		<−25	−28
GLN	P4		−23	−25
ASP^{-1}	Qa		<−25	–
ASP^{0}	P3		−18	−19
GLU^{-1}	Qa		<−25	–
GLU^{0}	P1		−11	−11
ARG^{+1}	N0-Qd	N0: Cβ-Cγ-Cδ-Nε	<−25	–
ARG^{0}	N0-P4	Qd/P4:Cζ-Nω1-Nω2	−23	−25
LYS^{+1}	C3-Qd	C3: Cβ-Cγ-Cδ	<−25	–
LYS^{0}	C3-P1	Qd/P1:Cε-Nω	−1	−2
HIS	SC4-SP1-SP1	SC4: Cβ-Cγ SP1: Cδ-Nε SP1: Nδ-Cε	−19	−20
PHE	SC4-SC4-SC4	SC4: Cβ-Cγ-Cδ1 SC4: Cδ2 -Cε2 SC4: Cε1-Cζ	19	17
TYR	SC4-SC4-SP1	SC4: Cβ-Cγ-Cδ1 SC4: Cδ2 -Cε2 SP1: Cε1-Cζ-OH	−1	−2
TRP	SC4-SP1-SC4-SC4	SC4: Cβ-Cγ-Cδ2 SP1: Cδ1-Nε1-Cε1 SC4: Cε2-Cζ2 SC4: Cε1-Cω	12	9

The experimental partitioning free energies are obtained for cyclohexane/water, the simulation results for butane/water, using Eq. 7. All values are expressed in kJ/mol and obtained at $T = 300$ K
[a]The mapping is reported only for amino acid side chains composed of more than one bead

dihedral and angle parameters are used to distinguish a helix, a strand, or a random coil. It is therefore not possible to study realistic folding-unfolding events at this stage.

Furthermore the structural SS parameters were extracted from a statistical analysis of protein structures and thus describe ideal secondary structure elements, e.g., α-helices and β-sheets. Note that this may result in an unusually high RMSD of the model with respect to the experimental structure but does not mean it is unfolding. In cases where the specificity of the local deformations of the protein backbone (e.g., helix kinks) is of interest the use of the elastic network together with the Martini model (ElNeDyn) is recommended (16). The elastic network defines a network of springs between backbone beads. We have shown that with an appropriate set of values for the cutoff distance limiting the extend of the network and of the force constant of the springs this model is able to simultaneously reproduce global and local deviations, fluctuations, as well as collective motions of all-atom protein models (16). It is of importance to note that since in this version of the protein force field the backbone bead is placed on the Cα atom all bonded parameters (equilibrium values and force constants) have been reparameterized accordingly (16).

Carbohydrates: The parameterization of carbohydrates followed the same philosophy as was used previously for lipids and proteins, focusing on the reproduction of partitioning free energies of small compounds between polar and non polar phases (42). The carbohydrate building blocks considered are the monosaccharides glucose and fructose, and the disaccharides sucrose, trehalose, maltose, cellobiose, nigerose, laminarabiose, kojibiose, and sophorose. For a single sugar ring (consisting of 12 nonhydrogen atoms) three CG particles are used. This level of resolution preserves the general mapping procedure for the Martini force field (4/1 mapping), the geometrical shape of the rings, and allows for a distinction between different types of monosaccharides through variation in the bond lengths, angles, and CG particle types. The particle types that best reproduced experimental partitioning data were found to be the polar class (P1–P4) of particles. Disaccharides are modeled as two to three bead units connected by a single bond, which mimics the glycosidic linkage. This geometry allows the definition (and subsequent parameterization) of the important φ and ψ dihedral angles, which determine the relative orientation and flexibility of the two sugar residues. The set of fine-grained particles represented by the CG beads is chosen to be different for the monosaccharide and the corresponding disaccharide residue. This somewhat non-obvious choice is based on the ability to represent the typical polar/apolar character of the disaccharides, with the apolar part corresponding to the central part along the glycosidic linkage. Oligosaccharides are constructed adding disaccharide residues through additional bonds. Bonded parameters for these saccharides were optimized by comparison to conformations sampled with an atomistic force field. Special attention was given to the

representation of the rotameric states. Applications of the carbohydrate model to the oligosaccharides amylose and curdlan show a preservation of the main structural properties, with three orders of magnitude more efficient sampling than the atomistic counterpart. The investigation of the cryo- and anhydroprotective effect of glucose and trehalose on a lipid bilayer showed a strong decrease of the melting temperature, in good agreement with both experimental findings and atomistic simulation studies (42).

3.2. Polarizable Water Model

The classic Martini water model does not bear charges and, consequently, is blind to electrostatic fields and polarization effects. A uniform screening is used instead. While this is a reasonable approximation for the bulk water, problems arise at interfaces between water and other phases and in the presence of charged particles. In our constant effort to improve the accuracy and the range of applicability of the Martini force field, a water model providing a better representation of the electrostatic interaction has been recently developed (31). It includes orientational polarizability by means of a dipole described by two net charges attached to the water bead, which carries the LJ potential (see Fig. 2a). The parameterization of the model followed three criteria: (1) The dielectric constant and (2) particle density of the model should be close to that of real water, and (3) the partitioning free energies between water and organic solvents, one of the cornerstones of the Martini model, should remain unaffected. The final polarizable model has a dielectric constant of 75.6, a density of 1,043 kg/m^3 and adjustments of its LJ parameters allowed to reproduce the right solvation energies for most particles. The LJ self- and cross-interactions of charged particles were modified to compensate for the important change in their interaction with the water model. Details of the model can be found elsewhere (31). Note that a model similar in spirit was published around the same time by Wu et al. (43).

While preserving many important properties of the classical Martini water model, the polarizable version significantly improves others. To illustrate the benefit of incorporating orientational polarization in the CG water model electroporation events were studied (31). It was notably shown that both poration of an octane slab in water under an external electric field and the poration of a lipid bilayer due to the electric field created by an ionic imbalance across the membrane are phenomena described realistically by the model. In Fig. 2c an example of the electroporation due to an unbalance of ion concentration is shown. A large water pore is spontaneously formed allowing the ions to cross the membrane bilayer. When the ion concentrations are equivalent on both sides of the bilayer the pore closes. The effect of the polarizable water model is more clearly seen in the snapshot presented in Fig. 2d,

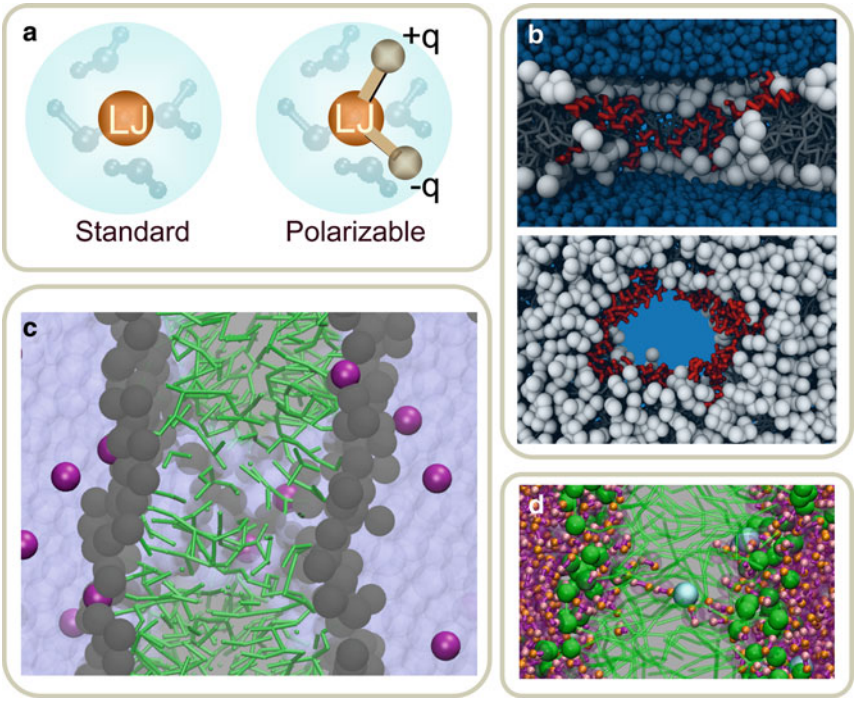

Fig. 2. New polarizable water model for Martini. The polarizable water model is shown in panel **a** together with the standard water model. In panel **b**, a transmembrane pore formed by magainin peptides is shown from the side (*top*) and the top (*bottom*) of the lipid bilayer. For clarity, in the side view the water is shown on both sides of the lipid bilayer and hidden in the transmembrane region; in the top view the water is not shown. In panel **c**, a water pore formed due to the presence of an ion gradient across the lipid bilayer is shown. The lipid head groups are depicted by *gray spheres* and the tail by *sticks*. The ions are the *solid spheres* and cross the membrane through the pore. In panel **d**, the dipoles of the polarizable water molecules are shown when solvating an ion upon crossing the membrane at low electric field. The water dipoles clearly orient due to the presence of the ion.

where a single ion permeated the membrane under a low electric field. During the permeation process, the ion keeps being hydrated to avoid the cost of desolvation in a low dielectric medium. The polarizable waters reorient in such a way that their dipoles stabilize the ionic charge. Another example of the potential range of applications with the polarizable water model is the formation of transmembrane pores by antimicrobial peptides. Although pores are formed with the nonpolarizable water model when self-assembly simulations are used (i.e., starting from randomly distributed systems), it was not possible to observe their formation on a preformed lipid bilayer. With the polarizable water model when a number of magainin peptides are added in the aqueous phase next to a DMPC bilayer, spontaneous pore formation is observed as is illustrated in Fig. 2b. The pore is of a disordered toroidal nature, in agreement with previous results from atomistic simulations (44, 45).

3.3. Specific Topologies

Nanomaterials: Fullerenes are molecules entirely composed of carbon atoms forming hollow spheres, ellipsoids, or tubes. They are products emerging from the development and use of nanomaterials and their effect on health and environment has become a concern. Monticelli and coworkers (46) have determined the topology of the C60 molecules based on a large collection of experimental data including its partitioning behavior in different solvents. The fullerenes are described by 16 CG beads, staying close to a 4/1 mapping, based on the bead type for benzene (SC4). This topology was used to describe the thermodynamics and mechanism of interaction of fullerene aggregates—C60 aggregates formed in aqueous solution—with a lipid bilayer (46). The authors primarily observed a complete dissolution of the fullerene aggregates into the lipid bilayer and noted to their surprise only relatively little mechanical damage of the bilayer. Carbon nanotubes (CNTs) are of great interest in a wide range of potential applications but still only little is known concerning their behavior in biological environment. Wallace and Sansom have built carbon nanotube (CNT) topologies using C-type particles from an earlier version of Martini (9). The model was used to study the interaction between CNT and several detergents with the aim of reducing CNT self-affinity and disperse them in an aqueous environment (47, 48). They also looked at the response of a lipid bilayer upon the penetration of CNTs of different radius and with different orientations relative to the membrane plane (49).

Collagen: Collagen molecules are abundant proteins in the human body where their mechanical properties provide stability, elasticity and strength to connecting tissues. A collagen topology (50) was built as an extension to the Martini protein force field. Collagen molecules are repeats of the GXY motif where X and Y may be any residue but often prolines and hydroxyprolines. They adopt a peculiar right-handed triple helix with a backbone conformation that was not yet available in the Martini force field. The authors defined a set of bonded terms (bond, angles and dihedrals) based on collagen experimental structures (for reference values) and atomistic simulations of small building blocks (for force constants). The hydroxyproline (hP) was first defined using the Black and Mould hydrophobicity scale to determine the most appropriate bead type (C5-P1) for its nonbonded interactions. The model was finally tested by calculating some mechanical features of the collagen molecule $[(\text{G-P-hP})_{10}]_3$. The Young's modulus and persistence length of the model were found in good agreement with experimental and computational values in the literature.

DNA: Double stranded DNA may mix with lipids to form lipoplexes. These have become attractive as they present a very promising alternative to viral gene vectors for the intracellular gene delivery. Their primary advantage being to have a lower toxicity to their host, but they are still not as efficient. Computer

simulations might help improving this formalism. Khalid and coworkers (51) have developed a coarse-grained model of DNA compatible with the Martini force field. The authors use Nd, Na and Nda particle types to describe the bases; the phosphate and deoxyribose groups are described by a Qa and C-Na bead type, respectively. Bonded terms were not a particular issue since an elastic network was used to connect all particles within 0.7 nm by a spring with a 1,500 kJ/mol/nm^2 force constant. The persistence length of the model was tuned in agreement with experimental values. The model was not tested further against experimental or computational data (51). The authors studied the nanoarchitecture of lipoplexes (52), which has been suggested to influence their efficiency, and were able to observe phase transitions and stability of large lipoplexes that were compatible with results obtained by SAXS.

Polymers: The use of CG models to describe polymer dynamics antedates the use of such models for lipid dynamics (53). Yet there is a need also for Martini models for polymeric systems, especially since it would then be possible to simulate systems in which polymers interact with biomolecules, which are already defined in Martini. One example is the use of dendrimers as efficient drug carriers for transmembrane cargo delivery. A Martini model for dendrimers was developed by Lee and Larson (54) who studied pore formation by polyamidoamine (PAMAM) dendrimers in DMPC and DPPC bilayers. Third and 5th generation dendrimers interact with DPPC and may cause pore formation depending on the chemical details of the dendrimers and the salt concentration (54). In a follow-up study (55), 5th and 7th generation dendrimers were simulated and showed distinct behavior depending on their charges, in agreement with atomic force microscopy experiments. Relatively subtle differences in structure caused significant differences in pore formation and water permeation through the bilayer, suggesting that the CG simulations are accurate enough to help design and understand this type of molecules (55). Other polymers with a large range of bioapplications are polyethylene oxide (PEO) and polyethylene glycol (PEG). They have in particular been conjugated to an array of pharmaceuticals to overcome limitations of low solubility, short circulating lifetime, and immunogenicity. The Martini model was recently parameterized for PEO and PEG (56). Based on reproducing structural properties such as the swelling in aqueous solution, the particle type for the C-O-C repeat unit was set to SNa. However, in order to reproduce the appropriate density of the melt, the self-interaction was somewhat increased. Another polymer for which Martini parameters are now available is polystyrene (57).

3.4. How to Make Your Own Topology

Here we present a simple three-step recipe, or guide, on how to proceed in parameterizing new molecules using the Martini model. The first step consists of mapping the chemical structure to the CG representation, the second step is the selection of appropriate

bonded terms, and the third step is the optimization of the model by comparing to AA level simulations and/or experimental data.

Step I, mapping onto CG representation: The first step consists in dividing the molecule into small chemical building blocks, ideally of four heavy atoms each. The mapping of CG particle types to chemical building blocks, examples of which are presented in Table 1, subsequently serves as a guide towards the assignment of CG particle types. Because most molecules cannot be entirely mapped onto groups of four heavy atoms, some groups will represent a smaller or larger number of atoms. In fact, there is no reason to map onto an integer number of atoms, e.g., a pentadecane mapped onto four C1 particles implies that each CG bead represents 3.75 methyl(ene) groups. In case of more substantial deviations from the standard mapping scheme, small adjustments can be made to the standard assignment. For instance, a group of three methyl(ene)s is more accurately modeled by a C2 particle (propane) than the standard C1 particle for saturated alkanes. The same effect is illustrated by the alcohols: whereas the standard alcohol group is modeled by a P1 particle (propanol), a group representing one less carbon is more polar (P2, ethanol), whereas adding a carbon has the opposite effect (Nda, butanol). Similar strategies can be used for modulation of other building blocks. To model compounds containing rings, a more fine-grained mapping procedure can be used. In those cases, the special class of S-particles is appropriate.

Step II, selecting bonded interactions: For most molecules the use of a standard bond length (0.47 nm) and force constant of $K_b = 1{,}250$ kJ/mol/nm^2 appears to work well. In cases where the underlying chemical structure is better represented by using different values, there is no restriction in adjusting these values. Especially for ring structures, much smaller bond lengths are required. For rigid rings, the harmonic bond and angle potentials are replaced by constraints, as was done for benzene and cholesterol. For linear chain-like molecules, a standard force constant of $K_a = 25$ kJ/mol with an equilibrium bond angle $\varphi_a = 180^\circ$ best mimics distributions obtained from fine-grained simulations. The angle may be set to smaller values to model unsaturated *cis*-bonds (for a single *cis*-unsaturated bond $K_a = 45$ kJ/mol and $\varphi_a = 120^\circ$) or to mimic the underlying equilibrium structure more closely in general. In order to keep ring structures planar, improper dihedral angles should be added. For more complex molecules (e.g., cholesterol), multiple ways exist for defining the bonded interactions. Not all of the possible ways are likely to be stable with the preferred time step of ~30 fs. Some trial-and-error testing is required to select the optimal set.

Step III, refinement: The coarse-graining procedure does not have to lead to a unique assignment of particle types and bonded interactions. A powerful way to improve the model is by comparison to

AA level simulations, analogous to the use of quantum calculations to improve atomistic models. Structural comparison is especially useful for optimization of the bonded interactions. For instance, the angle distribution function for a CG triplet can be directly compared to the distribution function obtained from the AA simulation, using the mapping procedure described earlier. The optimal value for the equilibrium angle and force constant can thus be extracted. Comparison of thermodynamic behavior is a crucial test for the assignment of particle types. Both AA level simulations (e.g., preferred position of a probe inside a membrane) and experimental data (e.g., the partitioning free energy of the molecule between different phases) are useful for a good assessment of the quality of the model. The balance of forces determining the partitioning behavior can be very subtle. A slightly alternative assignment of particle types may significantly improve the model. Once more, it is important to stress that Table 1 serves as a guide only; ultimately the comparison to AA simulations and experimental data should be the deciding factor in choosing parameters.

During the refinement of the bonded and nonbonded terms of the CG topology of a molecule, one should keep in mind that these terms are strongly interdependent. When associating two or more beads together the principle of additivity of solvation free energy (and therefore partitioning free energy) may be followed as a first approximation. But this will not hold in many situations. For instance in a molecule when the distance between two beads is set to one smaller than the standard 0.47 nm (close to the particle LJ diameter: 0.526 nm) their association will result in an overlap of their LJ spheres and thereby reduce the volume of the molecule as a whole when compared to the sum of the bead sizes. As a result, the solvation free energy of the molecule will be larger than the sum of the values for each bead and thus will be overestimated. This is due to the loss of the energy cost of generating a cavity to fit the overlapping section(s) of the molecule in the solvent. This effect may be as large as 10–15 kJ/mol when the distance is decreased from 0.47 to 0.25 nm.

4. Applications

The list of applications of the Martini model to date is broad, reflecting the flexibility and transferability underlying our coarse-graining protocol. Some important applications include, among others, (protein mediated) vesicle fusion (58–61), lamellar phase transformations (19–21, 39), the collapse of monolayers (62–64), peptide-induced membrane modulation (65–68), the self-assembly of membrane-proteins (15, 18, 26, 27, 29, 69–71), gating of proteins (72–76), carbon nanotube-lipid interactions (46, 49),

confinement of copolymers (77), structure and dynamics of lipoprotein particles (26, 27, 40), pore formation by dendrimers (54, 55, 78), and formation of lipoplexes (52). In most of these studies the CG model, sometimes with small changes or extensions from the published version, performed well when compared to either experimental data or to more detailed atomistic models. Here we selected three applications of ongoing studies performed in our own lab, namely, simulations of raft-like lipid membranes, gating of mechanosensitive channels, and the involvement of cardiolipins in the formation of membrane protein supercomplexes. All simulations were performed with the GROMACS simulation software (23), versions 4.0. In the applications, we will use an effective time rather than the actual simulation time to account for the speed-up in coarse-grained dynamics (see Subheading 2.4).

4.1. Molecular Face of Lipid Rafts

The lateral heterogeneity of biological membranes has important implications for the function of cells. Nevertheless, to study the organization of biological membranes remains a challenge, because it is inherently difficult to characterize fluctuating nanoscale assemblies in living cells. Model membranes and isolated plasma membranes are more frequently studied, because large-scale phase separation can occur in these systems (79–81). In particular, ternary mixtures of saturated lipids, unsaturated lipids, and cholesterol can segregate into two coexisting fluid lipid domains, a liquid-ordered (Lo) and liquid-disordered (Ld) phase. The Martini model has proven very useful to assess the molecular nature of these domains at the nanoscale, information that has thus far eluded experimental determination. We have been able to show the spontaneous separation of a saturated phosphatidylcholine (PC)/unsaturated PC/cholesterol mixture into a liquid-ordered and a liquid-disordered phase with structural and dynamic properties closely matching experimental data (22). The lipid bilayer used in this study consisted of a ternary mixture of saturated di-C16:0PC (dipalmitoyl-phosphatidylcholine, DPPC), doubly unsaturated di-C18:2PC (dilinoleoyl-phosphatidylcholine, DLiPC), and cholesterol (molar ratio 0.42:0.28:0.3). The near-atomic resolution of the simulations reveals remarkable features of both domains, and of the boundary domain interface. Furthermore, we predicted the existence of a small surface tension between the monolayer leaflets, which drives registration of the domains. At the level of molecular detail, raft-like lipid mixtures show a surprising face with possible implications for many cell membrane processes (22).

It is intriguing to devise molecules that specifically bind at the boundary interface between the different lipid domains, thereby modifying the boundary properties while leaving the bulk regions unaltered. As they are supposed to reduce the line tension (or energetic cost) of the one-dimensional boundary interface, such molecules can be called linactants, analogous to surfactants (which

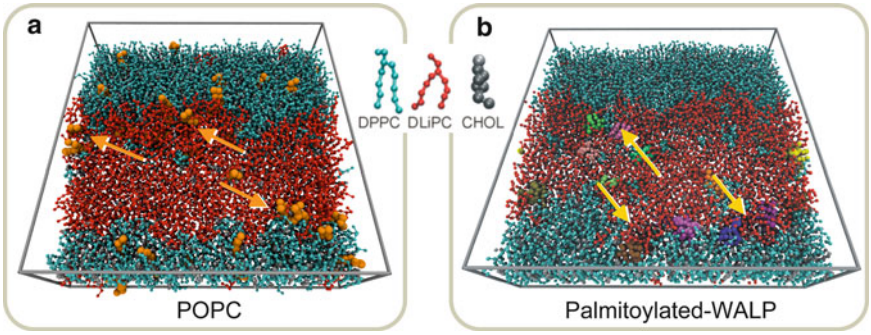

Fig. 3. Prediction of linactant behavior in multicomponent lipid membranes. Simulation snapshots of a ternary lipid mixture (DPPC/DLiPC/Cholesterol) to which a minor fraction (2 mol%) of a fourth component has been added that prefers to be at the domain boundary between the liquid-ordered and liquid-disordered phases. In panel **a**, the fourth component is POPC, a hybrid lipid with one saturated and one unsaturated tail. In panel **b**, the fourth component is a double-palmitoylated WALP peptide. *Arrows point* at a few individual molecules residing at the domain boundary, i.e., to be linactive.

modify the surface tension at an oil–water interface) (82). Possible line-active molecules could be, e.g., certain lipids, or lipid-anchored or transmembrane proteins. Recently we simulated the partitioning of other lipids as well as of transmembrane helices in the ternary mixture described above (65, 83). To this ternary mixture, small amounts of the fourth component were added. The idea was to introduce enough molecules to obtain proper statistics during the MD simulation, while perturbing the phase diagram of the ternary system as weakly as possible. Figure 3a shows typical line-active behavior of a palmitoyloleoyl-phosphatidylcholine (POPC) lipid. POPC, with both a saturated and an unsaturated tail, does not like either the Ld or the Lo phase, and has a tendency to accumulate at the domain boundary interface. In doing so, the line tension between the domains is reduced by about 30%, a strong effect given the low overall concentration of the POPC lipid (2 mol%). Similar line-active behavior was also observed for lyso-PC, a lipid with only one tail. In the case of TM peptides, most peptides studied, irrespective of hydrophobic matching conditions, have a strong preference for the Ld phase. Free energy calculations show that the enthalpic contribution due to the packing of the lipids drives the lateral sorting of the helices. In the Lo phase, the lipids are packed tightly together with cholesterol; this packing is distorted in the presence of a TM helix. The Ld phase, which is disordered, can accommodate the peptide with less impact on the lipid packing interactions. To drive peptides to the Lo phase, lipid anchors are required. Figure 3b shows the distribution of model TM peptides (WALPs) with multiple saturated lipid tails attached. The peptides cluster near the Lo/Ld domain boundary. Without the anchors, WALP is only found in the Ld phase.

4.2. Mechanosensitive Channels in Action

Mechanosensitive channels form transmembrane pores to counteract pressure gradient buildup by balancing the osmotic conditions on either side of the cell membrane (84, 85). When activated, e.g., by increased membrane tension, the mechanosensitive channel of large conductance (MscL) forms a nonselective transmembrane channel capable of quickly transporting large amounts of solvent and solutes. MscLs are usually active no longer than a few hundreds of milliseconds with characteristic, rapidly flickering activation–deactivation cycles plainly visible in single-channel traces. By introducing ingenious point-mutations (86) at the channel walls the activation and deactivation of MscL can be controlled by ambient pH and/or light (87). This makes MscL a functional nanovalve with engineerable properties for a rapid, targeted drug release from a suitable nanocontainer (e.g., a stable liposome) acting as a drug delivery vehicle. MscL is a pentamer and each of the five subunits consists of a transmembrane and a cytoplasmic domain connected by a flexible linker (Fig. 4). The two transmembrane helices TM1 and TM2 and the N-terminal helix S1 are arranged in a crisscross manner with

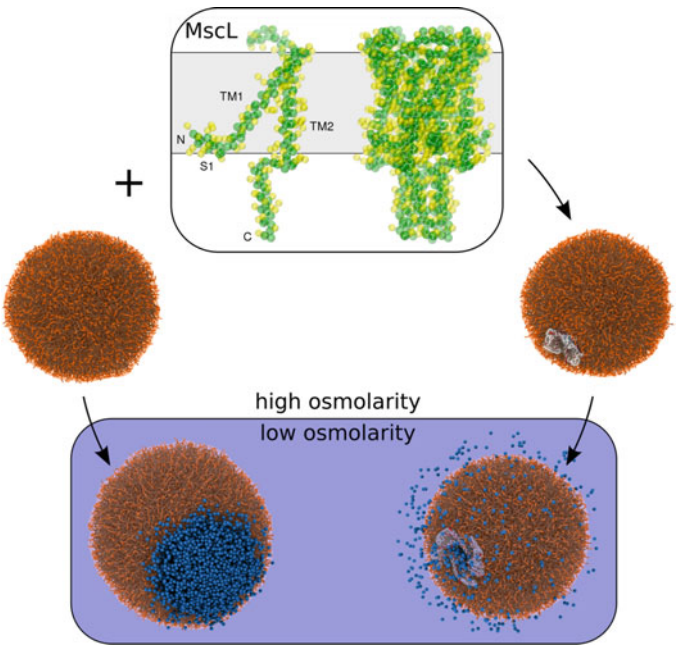

Fig. 4. Release of contents from pressurized liposomes. Response of a vesicle to a change in osmolarity with (*right*) and without (*left*) the presence of a mechanosensitive channel of large conductance (MscL). The MscL structure is shown in the *top panel*. One can appreciate the structure of a single subunit (*left*) and of the pentamer (*right*). The *gray area* represents the transmembrane region. *Left path*: an osmotic shock causes the vesicle to swell and ultimately to pop when its elastic limit is reached. *Right path*: under the same conditions but in the presence of an MscL the vesicle will survive by releasing the excess solvent (*small spheres*) through the opened channel.

TM1 and TM2 passing through the membrane, and S1 parallel to the membrane surface (Fig. 4). The transmembrane complex forms a ring-like structure with a hydrophobic lock region located slightly towards the cytoplasmic side from the center of the membrane. The cytoplasmic domains form a helical bundle at the mouth of the membrane channel.

The spontaneous gating of an MscL channel was studied using the Martini force field (10, 14). Originally, a lamellar setup was chosen (72), but more recently the gating of the channel in a small liposome was simulated (73). Simulations were carried out starting from the crystal structure of an MscL in its closed state (88) immersed in a small dioleoylphosphatidylcholine (DOPC) lipid vesicle measuring ~16 nm in diameter. Subsequently, a hypoosmotic shock condition was mimicked by gradually increasing the internal water content, and hence interior pressure, of the vesicle over a 0.5 μs time window. Following the evolution of this system (over 10s of microseconds) under such a stress condition and comparing it to the case of a vesicle lacking the embedded MscL (cf. Fig. 4) it was found that (1) MscL activates at the limit of membrane elasticity, thereby releasing internal pressure and preventing membrane disruption; (2) The opening mechanism is asymmetric: the five subunits do open simultaneously but independently to accommodate the change in membrane thickness; (3) Flow of water through the channel is bi-directional; (4) Liposomal stress is relaxed on a submillisecond time scale. More details can be found elsewhere (73).

4.3. Mitochondrial Supercomplex Formation

Mitochondria are intracellular organelles, which are the power plants of most eukaryotic cells. The energy is produced in the oxidative phosphorylation (OxPhos) system and results from a series of electron transfer (oxidoreduction reactions) mainly carried out by four large membrane protein assemblies, the so-called respiratory chain complexes eukaryotic (I–IV) and by some small electron carriers (quinones and cytochrome c). The tortuous electron path through the respiratory chain triggers the transport of protons from the inside to the outside of the mitochondrial inner membrane, leading to an electrochemical gradient, which is used by the ATP synthase complex (complex V) for ATP synthesis. The respiratory chain complexes I–IV self-organize into supramolecular structures called respiratory "supercomplexes" (RSC) or "respirasomes" (89, 90). Examples are the supercomplexes consisting of complexes III and IV ($III_2 + IV_1$ and $III_2 + IV_2$) and even larger complexes additionally including complex I ($I_1 + III_2 + IV_n$). While the existence and stoichiometry of supercomplexes has been established for a few organisms, the detailed structure (e.g., interfaces between complexes within supercomplexes) and most importantly the putative functional role and dynamics of those supercomplexes remains unclear. Notably, lipid membrane composition has been shown to be of great importance for the formation and stability of the

supercomplex III_2 + IV_2, and to have functional consequences. In that matter, cardiolipins (CLs), which compose 10–20% of the mitochondrial inner membrane, have been shown to be of primary importance (91–93). It is however not clear from the current experimental data by which mechanism CL might operate. Although cocrystallized CLs are found close to the surface of the protein in the transmembrane domain they are located deep inside a cavity and a helical subunit prevents them from having contact with bulk lipids and other embedded proteins.

Simulations of Martini models of complex III_2 and IV embedded in a lipid membrane of POPC molecules containing ~20% cardiolipins were performed (94) and revealed preferential interfaces of CLs for both complexes III_2 and IV (see Fig. 5). It is important to note that long simulations (10s of microseconds) were needed to reach acceptable convergence of the interfaces. Most interestingly, these actual *binding sites* differ significantly from the positions of CLs found in the crystal structures: they are at the surface of the proteins and not buried within the complexes. Furthermore self-assembly simulations of complexes III_2 and IV in the presence of CLs showed that in the supercomplexes formed: (1) complexes conserve all the binding sites observed in the simulations when isolated; (2) supercomplexes make contact through those binding sites and therefore the binding sites are shared by the complexes. A typical example of a supercomplex formed is shown in Fig. 5d. These findings clearly show that bulk CLs strongly bind to the surface of the complexes reproducibly at specific locations and thereby provide anchors to form contacts with other complexes. Although this view contrasts with the earlier ideas that buried CLs were important for the formation of supercomplexes it allows the rationalization of the effect of the lack of cardiolipins on the formation of supercomplexes in a more intuitive and straightforward manner. Ongoing research in our laboratory aims at determining the precise role of the different sites and their degree of occupation in orienting the complexes relative to each other.

5. Outlook

In line with our constant efforts in improving the Martini coarse-grained force field and its range of applicability a few directions of development are currently being followed.

New nonbonded form: The use of a LJ 12-6 potential to describe the nonbonded interactions is, on hindsight, not the best choice. The steep repulsion leads to overstructuring of the Martini model in comparison to atomistic models, as evidenced for instance in the radial-distribution functions for simple alkanes (13). To reproduce

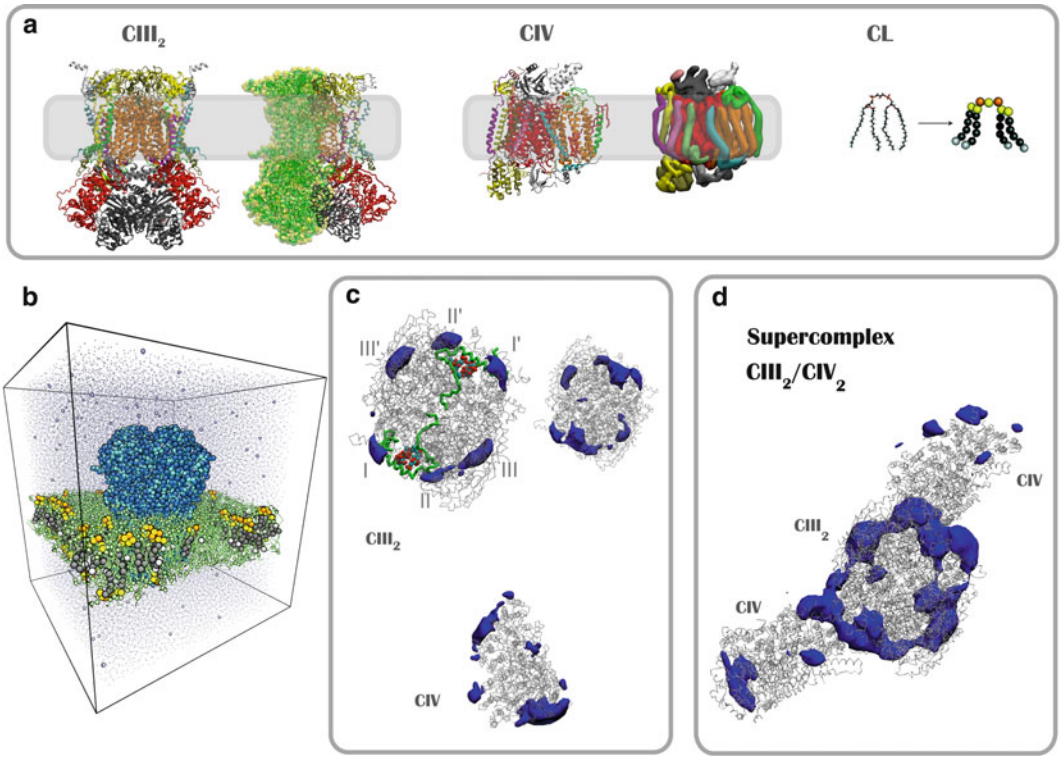

Fig. 5. Cardiolipins control mitochondrial supercomplex structure. The atomistic structures of complex-III homodimer ($CIII_2$), complex-IV (CIV) and cardiolipins (CL) are shown in panel **a** together with their CG representation. In the case of $CIII_2$ and CIV a few representations are used. One monomer of $CIII_2$ is shown using vdW spheres. The second monomer is shown using a stick representation of the backbone (Cα) trace. The CIV CG model is represented by the density of the backbone beads obtained during a simulation. In panel **b** a typical system is shown. Here the $CIII_2$ is embedded into a POPC membrane bilayer with 20 % of cardiolipins (*solid*). The aqueous phase is shown by small dots (*water beads*). Solvated ions are represented by spheres. In panel **c**, $CIII_2$ (*top*) and CIV (*bottom*) are shown by gray transparent surfaces. The *solid* surfaces represent the regions of the system with high density of CLs. In panel **d**, an example is shown of the structure of the supercomplex $CIII_2$–CIV_2 as obtained by a self-assembly simulation. The solid surfaces represent the regions of the system with high density in CLs. The orientation of CIII2 in panels **c** and **d** is kept identical to ease the comparison of the CL high density regions in the individual complexes (panel **c**) and in the supercomplex.

the "softness" of real systems a power 9 or 10 repulsive term appears more appropriate, as in the recently reparameterized CG model of Klein and coworkers (95) that uses a LJ 9-6 form for most non-bonded interactions. The other drawback of the LJ 12-6 potential is the limited fluid range (see Subheading 2.4), preventing for instance the accurate reproduction of the experimental surface tension of hydrophilic compounds, including water. Possible solutions are given in the literature, such as switching to a power 4 attraction (96, 97), or to a different potential such as the Morse potential (98). For the Martini version 3.x we aim to change the nonbonded form to a softer potential with longer-ranged attraction.

Foldable peptides and proteins: The lack of structural flexibility of the current Martini protein backbone (see Subheadings 2.4 and 3) obviously limits the range of applicability of the model. While aiming at a coarse-grained model capable of folding a protein from its sequence may be overly ambitious, describing the backbone in a more realistic manner would be an appreciable improvement. For instance modeling the formation and realistic transition between secondary structure elements would be extremely beneficial. Available coarse-grained models for protein represent the backbone H-bonding in quite different manners and generally use a specific potential (74, 99–103). In contrast we want to keep a simple and generic. For instance, we have been exploring the possibility of using a fixed dipole (by the mean of two point charges of opposite sign) to represent the backbone polarity. The dipoles interact with other dipoles and particles through regular Coulomb and LJ potentials. Importantly, this description restores the directionality of backbone interactions. We have recently demonstrated proof of concept for generic polypeptides in the sense that secondary structure elements (α-helices and β-sheets) may form, be stable and interconvert. The simplicity of the model allows easy tuning of the propensity of the backbone of each residue between extended and compact structures. This might be convenient if one wants to assign a certain preference for secondary structure at the residue level.

Nucleotides: One of the major classes of biomolecules that has not been thoroughly parameterized for Martini is the nucleotides, and the DNA and RNA molecules they constitute. Although there is a Martini model available for a small piece of DNA (51), a more generic approach is required to make the model applicable to all nucleic acids. We plan to perform such a parameterization analogous to our work on carbohydrates (42) described above. We will start with optimizing the description of the eight main nucleotides, focusing on thermodynamic partitioning behavior to select the best particle types, and comparing to atomistic simulations to select the bonded interactions. Subsequently we will consider conformational behavior of small oligonucleotides. Tuning of bonded parameters (angle and dihedral) will be used to result in mimicking the flexibility observed with atomistic models. The model can then be used to simulate large fragments of nucleic acids. Potentially an elastic network may be added (such as the ElNeDyn approach we developed for proteins) to assure a realistic behavior.

Multiscaling: In combination, FG and CG models are even more powerful. One of the current challenges is to develop effective multiscale methods (104, 105), which combine the advantages of both levels of resolution. A useful, serial type of multiscaling is the method of resolution transformation in which a CG configuration is back-mapped to an atomistic one. We have developed a

simple simulated-annealing based algorithm that can be used to perform resolution transformation for an arbitrary system (106). A subsequent simulation of the system with an atomistic force field allows one to assess, to some extent, the relevance of the configuration sampled at the CG level (107). A potentially powerful way to combine FG and CG force fields in parallel, is to define a specific region of interest to be modeled atomistically, whereas the rest of the system is described at the CG level. This so-called boundary approach, with a fixed separation between the two regions, is analogous to the idea of QM/MM methods in which quantum mechanics is combined with classical molecular mechanics. Exploratory work on boundary multiscaling methods combining FG and CG models has already been performed by several groups (24, 108, 109). We recently proposed a novel variation of the boundary method that is more general and requires only few additional parameters (110). Instead of deriving specific cross-interactions, we use virtual sites that couple the atomistic and CG degrees of freedom. These virtual sites are constructed from the center-of-mass of the underlying all-atom representation. The hybrid particles constituting the central molecule thus interact intramolecularly using FG forces, and intermolecularly according to the CG forces. An advantage is that no specific interactions between FG and CG beads need to be parameterized as is done in other boundary methods (24), making the method easily applicable to any system of interest. The method naturally combines the advantages of FG models (accurate description of the molecule of interest) and CG models (explicit treatment of the surrounding solvent at a speed 2–3 orders of magnitude larger compared to FG models). So far, the method has only been tested for simple systems consisting of pure butane, or dialanine peptides in either water or butane (110) as a proof of principle. Any type of CG (and FG) force field can be used, and results obtained with combining the Martini force field to the GROMOS force field have especially been encouraging. Within the field of biomolecules, the method appears ideally suited to study e.g., protein–ligand binding, where the active site and ligand are modeled in atomistic detail and the rest of the protein, together with the solvent, is coarse-grained. The combination of a flexible protein description and explicit solvent is envisioned to be important for molecular docking approaches (111, 112). Another area of potential applications is the complexation of proteins, with the surface of the protein in full detail and the protein core as well as the surrounding solvent at the CG level. Finally, our method offers an alternative approach to arrive at a “foldable” Martini model (see above), with the protein backbone in full atomic detail and the side chains and solvent at a CG level.

Acknowledgments

The authors would like to thank the many people that have directly and indirectly contributed to the development of the Martini force field. In particular Alex de Vries and all the past and present members of the MD group in Groningen are acknowledged for their dynamism and enthusiasm in using, criticizing and improving Martini, as well as the groups of Peter Tieleman, Luca Monticelli, and Ilpo Vattulainen. Clement Arnarez, Martti Louhivuori, Lars Schafer, and Durba Sengupta provided data and images for the figures.

References

1. Smit B, Hilbers PAJ, Esselink K, Rupert LAM, Vanos NM, Schlijper AG (1990) Computer-simulations of a water oil interface in the presence of micelles. Nature 348:624–625
2. Muller M, Katsov K, Schick M (2006) Biological and synthetic membranes: what can be learned from a coarse-grained description? Phys Rep 434:113–176
3. Shillcock JC, Lipowsky R (2006) The computational route from bilayer membranes to vesicle fusion. J Phys-Condens Mat 18: S1191–S1219
4. Venturoli M, Sperotto MM, Kranenburg M, Smit B (2006) Mesoscopic models of biological membranes. Phys Rep 437:1–54
5. Elezgaray J, Laguerre M (2006) A systematic method to derive force fields for coarse-grained simulations of phospholipids. Comput Phys Commun 175:264–268
6. Lyubartsev AP (2005) Multiscale modeling of lipids and lipid bilayers. Eur Biophys J Biophy 35:53–61
7. Shelley JC, Shelley MY, Reeder RC, Bandyopadhyay S, Moore PB, Klein ML (2001) Simulations of phospholipids using a coarse grain model. J Phys Chem B 105:9785–9792
8. Izvekov S, Violi A, Voth GA (2005) Systematic coarse-graining of nanoparticle interactions in molecular dynamics simulation. J Phys Chem B 109:17019–17024
9. Marrink SJ, de Vries AH, Mark AE (2004) Coarse grained model for semiquantitative lipid simulations. J Phys Chem B 108:750–760
10. Marrink SJ, Risselada HJ, Yefimov S, Tieleman DP, de Vries AH (2007) The MARTINI force field: coarse grained model for biomolecular simulations. J Phys Chem B 111:7812–7824
11. Oostenbrink C, Villa A, Mark AE, Van Gunsteren WF (2004) A biomolecular force field based on the free enthalpy of hydration and solvation: the GROMOS force-field parameter sets 53A5 and 53A6. J Comput Chem 25:1656–1676
12. Chu JW, Ayton GS, Izvekov S, Voth GA (2007) Emerging methods for multiscale simulation of biomolecular systems. Mol Phys 105:167–175
13. Baron R, Trzesniak D, de Vries AH, Elsener A, Marrink SJ, van Gunsteren WF (2007) Comparison of thermodynamic properties of coarse-grained and atomic-level simulation models. Chem Phys Chem 8:452–461
14. Monticelli L, Kandasamy SK, Periole X, Larson RG, Tieleman DP, Marrink SJ (2008) The MARTINI coarse-grained force field: extension to proteins. J Chem Theory Comput 4:819–834
15. Sengupta D, Marrink SJ (2010) Lipid-mediated interactions tune the association of glycophorin A helix and its disruptive mutants in membranes. Phys Chem Chem Phys 12:12987–12996
16. Periole X, Cavalli M, Marrink SJ, Ceruso MA (2009) Combining an elastic network with a coarse-grained molecular force field: structure, dynamics, and intermolecular recognition. J Chem Theory Comput 5:2531–2543
17. Ramadurai S, Holt A, Schafer LV, Krasnikov VV, Rijkers DTS, Marrink SJ, Killian JA, Poolman B (2010) Influence of hydrophobic mismatch and amino acid composition on the lateral diffusion of transmembrane peptides. Biophys J 99:1447–1454
18. Periole X, Huber T, Marrink SJ, Sakmar TP (2007) G protein-coupled receptors self-assemble in dynamics simulations of model bilayers. J Am Chem Soc 129:10126–10132

19. Marrink SJ, Mark AE (2004) Molecular view of hexagonal phase formation in phospholipid membranes. Biophys J 87:3894–3900
20. Marrink SJ, Risselada J, Mark AE (2005) Simulation of gel phase formation and melting in lipid bilayers using a coarse grained model. Chem Phys Lipids 135:223–244
21. Faller R, Marrink SJ (2004) Simulation of domain formation in DLPC-DSPC mixed bilayers. Langmuir 20:7686–7693
22. Risselada HJ, Marrink SJ (2008) The molecular face of lipid rafts in model membranes. P Natl Acad Sci USA 105:17367–17372
23. Van der Spoel D, Lindahl E, Hess B, Groenhof G, Mark AE, Berendsen HJC (2005) Gromacs: fast, flexible, and free. J Comput Chem 26:1701–1718
24. Shi Q, Izvekov S, Voth GA (2006) Mixed atomistic and coarse-grained molecular dynamics: simulation of a membrane-bound ion channel. J Phys Chem B 110:15045–15048
25. Bowers KJ, Chow E, Xu HF, Dror RO, Eastwood MP, Gregersen BA, Klepeis JL, Kolossváry I, Moraes MA, Sacerdoti FD, Salmon JK, Shan Y, Shaw DE (2006) Scalable Algorithms for Molecular Dynamics Simulations on Commodity Clusters. Proceedings of the ACM/IEEE Conference on Supercomputing (SC06) Tampa, Florida
26. Shih AY, Arkhipov A, Freddolino PL, Schulten K (2006) Coarse grained protein-lipid model with application to lipoprotein particles. J Phys Chem B 110:3674–3684
27. Shih AY, Freddolino PL, Arkhipov A, Schulten K (2007) Assembly of lipoprotein particles revealed by coarse-grained molecular dynamics simulations. J Struct Biol 157:579–592
28. Bond PJ, Holyoake J, Ivetac A, Khalid S, Sansom MSP (2007) Coarse-grained molecular dynamics simulations of membrane proteins and peptides. J Struct Biol 157:593–605
29. Bond PJ, Sansom MSP (2006) Insertion and assembly of membrane proteins via simulation. J Am Chem Soc 128:2697–2704
30. Villa A, Mark AE (2002) Calculation of the free energy of solvation for neutral analogs of amino acid side chains. J Comput Chem 23:548–553
31. Yesylevskyy SO, Schafer LV, Sengupta D, Marrink SJ (2010) Polarizable water model for the coarse-grained MARTINI force field. PLoS Comput Biol 6:e1000810
32. Marrink SJ, Periole X, Tieleman DP, de Vries AH (2010) Comment on "On using a too large integration time step in molecular dynamics simulations of coarse-grained molecular models" by M. Winger, D. Trzesniak, R. Baron and W. F. van Gunsteren (2009) Phys. Chem. Chem. Phys, 11: 1934, Phys Chem Chem Phys 12: 2254–2256
33. Xing CY, Faller R (2009) Coarse-grained simulations of supported and unsupported lipid monolayers. Soft Matter 5:4526–4530
34. Yano Y, Matsuzaki K (2006) Measurement of thermodynamic parameters for hydrophobic mismatch 1: Self-association of a transmembrane helix. Biochem Us 45:3370–3378
35. Ash WL (2009) Helix-helix interactions in membrane proteins probed with computer simulations. PhD Thesis (University of Calgary, Canada).
36. Winger M, Trzesniak D, Baron R, van Gunsteren WF (2009) On using a too large integration time step in molecular dynamics simulations of coarse-grained molecular models. Phys Chem Chem Phys 11:1934–1941
37. Marrink SJ, de Vries AH, Harroun TA, Katsaras J, Wassall SR (2008) Cholesterol shows preference for the interior of polyunsaturated lipid. J Am Chem Soc 130:10–11
38. Bennett WFD, MacCallum JL, Hinner MJ, Marrink SJ, Tieleman DP (2009) Molecular view of cholesterol flip-flop and chemical potential in different membrane environments. J Am Chem Soc 131:12714–12720
39. Dahlberg M (2007) Polymorphic phase behavior of cardiolipin derivatives studied by coarse-grained molecular dynamics. J Phys Chem B 111:7194–7200
40. Vuorela T, Catte A, Niemela PS, Hall A, Hyvonen MT, Marrink SJ, Karttunen M, Vattulainen I (2010) Role of lipids in spheroidal high density lipoproteins. PLoS Comput Biol 6:e1000964
41. Bulacu M, Periole X, Marrink SJ. (2012) In-silico design of robust bolalipid membranes. Biomacromol 13:196–205
42. Lopez CA, Rzepiela AJ, de Vries AH, Dijkhuizen L, Hunenberger PH, Marrink SJ (2009) Martini coarse-grained force field: extension to carbohydrates. J Chem Theory Comput 5:3195–3210
43. Wu Z, Cui QA, Yethiraj A (2010) A New coarse-grained model for water: the importance of electrostatic interactions. J Phys Chem B 114:10524–10529
44. Leontiadou H, Mark AE, Marrink SJ (2006) Antimicrobial peptides in action. J Am Chem Soc 128:12156–12161
45. Sengupta D, Leontiadou H, Mark AE, Marrink SJ (2008) Toroidal pores formed by antimicrobial peptides show significant disorder. BBA-Biomembranes 1778:2308–2317

46. Wong-Ekkabut J, Baoukina S, Triampo W, Tang IM, Tieleman DP, Monticelli L (2008) Computer simulation study of fullerene translocation through lipid membranes. Nat Nanotechnol 3:363–368
47. Wallace EJ, Sansom MSP (2009) Carbon nanotube self-assembly with lipids and detergent: a molecular dynamics study. Nanotechnology 20:045101
48. Wallace EJ, Sansom MSP (2007) Carbon nanotube/detergent interactions via coarse-grained molecular dynamics. Nano Lett 7:1923–1928
49. Wallace EJ, Sansom MSP (2008) Blocking of carbon nanotube based nanoinjectors by lipids: A simulation study. Nano Lett 8:2751–2756
50. Gautieri A, Russo A, Vesentini S, Redaelli A, Buehler MJ (2010) Coarse-grained model of collagen molecules using an extended MARTINI force field. J Chem Theory Comput 6:1210–1218
51. Khalid S, Bond PJ, Holyoake J, Hawtin RW, Sansom MSP (2008) DNA and lipid bilayers: self-assembly and insertion. J R Soc Interface 5:S241–S250
52. Corsi J, Hawtin RW, Ces O, Attard GS, Khalid S (2010) DNA lipoplexes: formation of the inverse hexagonal phase observed by coarse-grained molecular dynamics simulation. Langmuir 26:12119–12125
53. Muller-Plathe F (2002) Coarse-graining in polymer simulation: from the atomistic to the mesoscopic scale and back. Chem Phys Chem 3:754–769
54. Lee H, Larson RG (2006) Molecular dynamics simulations of PAMAM dendrimer-induced pore formation in DPPC bilayers with a coarse-grained model. J Phys Chem B 110:18204–18211
55. Lee H, Larson RG (2008) Coarse-grained molecular dynamics studies of the concentration and size dependence of fifth- and seventh-generation PAMAM dendrimers on pore formation in DMPC bilayer. J Phys Chem B 112:7778–7784
56. Lee H, de Vries AH, Marrink SJ, Pastor RW (2009) A coarse-grained model for polyethylene oxide and polyethylene glycol: conformation and hydrodynamics. J Phys Chem B 113:13186–13194
57. Rossi G, Monticelli L, Puisto SR, Vattulainen I, Ala-Nissila T (2010) Coarse-graining polymers with the MARTINI force-field: polystyrene as a benchmark case Soft Matter 7:698–708
58. Marrink SJ, Mark AE (2003) The mechanism of vesicle fusion as revealed by molecular dynamics simulations. J Am Chem Soc 125:11144–11145
59. Kasson PM, Kelley NW, Singhal N, Vrljic M, Brunger AT, Pande VS (2006) Ensemble molecular dynamics yields submillisecond kinetics and intermediates of membrane fusion. P Natl Acad Sci USA 103:11916–11921
60. Baoukina S, Tieleman DP (2010) Direct simulation of protein-mediated vesicle fusion: lung surfactant protein B. Biophys J 99:2134–2142
61. Smirnova YG, Marrink SJ, Lipowsky R, Knecht V (2010) Solvent-exposed tails as prestalk transition states for membrane fusion at low hydration. J Am Chem Soc 132:6710–6718
62. Baoukina S, Monticelli L, Marrink SJ, Tieleman DP (2007) Pressure-area isotherm of a lipid monolayer from molecular dynamics simulations. Langmuir 23:12617–12623
63. Duncan SL, Larson RG (2010) Folding of lipid monolayers containing lung surfactant proteins SP-B1-25 and SP-C studied via coarse-grained molecular dynamics simulations. BBA-Biomembranes 1798:1632–1650
64. Baoukina S, Monticelli L, Risselada HJ, Marrink SJ, Tieleman DP (2008) The molecular mechanism of lipid monolayer collapse. P Natl Acad Sci USA 105:10803–10808
65. Schäfer LV, Marrink SJ (2010) Partitioning of lipids at domain boundaries in model membranes. Biophys J 99(12):L91–L93
66. Fuhrmans M, Knecht V, Marrink SJ (2009) A single bicontinuous cubic phase induced by fusion peptides. J Am Chem Soc 131:9166–9167
67. Polyansky AA, Ramaswarny PE, Volynsky PE, Sbalzarini IF, Marrink SJ, Efremov RG (2010) Antimicrobial peptides induce growth of phosphatidylglycerol domains in a model bacterial membrane. J Phys Chem Lett 1:3108–3111
68. Khalfa A, Tarek M (2010) On the antibacterial action of cyclic peptides: insights from coarse-grained MD simulations. J Phys Chem B 114:2676–2684
69. Bond PJ, Wee CL, Sansom MSP (2008) Coarse-grained molecular dynamics simulations of the energetics of helix insertion into a lipid bilayer. Biochem-Us 47:11321–11331
70. Psachoulia E, Fowler PW, Bond PJ, Sansom MSP (2008) Helix-helix interactions in membrane proteins: coarse-grained simulations of glycophorin a helix dimerization. Biochemistry 47:10503–10512

71. Sansom MSP, Scott KA, Bond PJ (2008) Coarse-grained simulation: a high-throughput computational approach to membrane proteins. Biochem Soc T 36:27–32
72. Yefimov S, van der Giessen E, Onck PR, Marrink SJ (2008) Mechanosensitive membrane channels in action. Biophys J 94:2994–3002
73. Louhivuori M, Risselada HJ, van de Rgiessen E, Marrink SJ (2010) Release of content through mechano-sensitive gates in pressurized liposomes. Proc Natl Acad Sci USA 107 (46):19856–19860. doi:10.1073/pnas.1001316107
74. Wei GH, Mousseau N, Derreumaux P (2004) Complex folding pathways in a simple beta-hairpin. Proteins 56:464–474
75. Treptow W, Marrink SJ, Tarek M (2008) Gating motions in voltage-gated potassium channels revealed by coarse-grained molecular dynamics simulations. J Phys Chem B 112:3277–3282
76. Lycklama JA, Bulacu M, Marrink SJ, Driessen AJM (2010) Immobilization of the plug domain inside the SecY channel allows unrestricted protein translocation. J Biol Chem 285:23747–23754
77. Hatakeyama M, Faller R (2007) Coarse-grained simulations of ABA amphiphilic triblock copolymer solutions in thin films. Phys Chem Chem Phys 9:4662–4672
78. Lee H, Larson RG (2008) Lipid bilayer curvature and pore formation induced by charged linear polymers and dendrimers: The effect of molecular shape. J Phys Chem B 112:12279–12285
79. Baumgart T, Hess ST, Webb WW (2003) Imaging coexisting fluid domains in biomembrane models coupling curvature and line tension. Nature 425:821–824
80. Veatch SL, Polozov IV, Gawrisch K, Keller SL (2004) Liquid domains in vesicles investigated by NMR and fluorescence microscopy. Biophys J 86:2910–2922
81. Lingwood D, Ries J, Schwille P, Simons K (2008) Plasma membranes are poised for activation of raft phase coalescence at physiological temperature. P Natl Acad Sci USA 105:10005–10010
82. Trabelsi S, Zhang S, Lee TR, Schwartz DK (2008) Linactants: Surfactant analogues in two dimensions. Phys Rev Lett 100:037802
83. Schäfer LV, de Jong DH, Holt A, Rzepiela AJ, de Vries AH, Poolman B, Killian JA, Marrink SJ (2010) Lipid packing drives the segregation of transmembrane helices into disordered lipid domains in model membranes. Proc Natl Acad Sci USA 108(4):1343–1348
84. Martinac B, Buechner M, Delcour AH, Adler J, Kung C (1987) Pressure-sensitive Ion channel in escherichia-coli. P Natl Acad Sci USA 84:2297–2301
85. Perozo E, Rees DC (2003) Structure and mechanism in prokaryotic mechanosensitive channels. Curr Opin Struc Biol 13:432–442
86. Kocer A, Walko M, Meijberg W, Feringa BL (2005) A light-actuated nanovalve derived from a channel protein. Science 309:755–758
87. Kocer A, Walko M, Feringa BL (2007) Synthesis and utilization of reversible and irreversible light-activated nanovalves derived from the channel protein MscL. Nat Protoc 2:1426–1437
88. Steinbacher S, Bass R, Strop P, Rees DC (2007) Structures of the prokaryotic mechanosensitive channels MscL and MscS. Curr Top Membr 58:1–24
89. Lenaz G, Genova ML (2009) Structural and functional organization of the mitochondrial respiratory chain: a dynamic super-assembly. Int J Biochem Cell B 41:1750–1772
90. Bultema JB, Braun HP, Boekema EJ, Kouril R (2009) Megacomplex organization of the oxidative phosphorylation system by structural analysis of respiratory supercomplexes from potato. BBA-Bioenergetics 1787:60–67
91. Zhang M, Mileykovskaya E, Dowhan W (2002) Gluing the respiratory chain together—Cardiolipin is required for supercomplex formation in the inner mitochondrial membrane. J Biol Chem 277:43553–43556
92. Zhang M, Mileykovskaya E, Dowhan W (2005) Cardiolipin is essential for organization of complexes III and IV into a supercomplex in intact yeast mitochondria. J Biol Chem 280:29403–29408
93. Pfeiffer K, Gohil V, Stuart RA, Hunte C, Brandt U, Greenberg ML, Schagger H (2003) Cardiolipin stabilizes respiratory chain supercomplexes. J Biol Chem 278:52873–52880
94. Arnarez C, Elezgaray J, Mazat JP, Marrink SJ, Periole X. Evidence for cardiolipin binding sites on the membrane exposed surface of the respiratory chain complex III. In preparation
95. Shinoda W, DeVane R, Klein ML (2010) Zwitterionic lipid assemblies: molecular dynamics studies of monolayers, bilayers, and vesicles using a new coarse grain force field. J Phys Chem B 114:6836–6849
96. Shinoda W, Devane R, Klein ML (2007) Multi-property fitting and parameterization of a coarse grained model for aqueous surfactants. Mol Simulat 33:27–36

97. DeVane R, Klein ML, Chiu CC, Nielsen SO, Shinoda W, Moore PB (2010) Coarse-grained potential models for phenyl-based molecules: I. Parametrization using experimental data. J Phys Chem B 114:6386–6393
98. Chiu CC, DeVane R, Klein ML, Shinoda W, Moore PB, Nielsen SO (2010) Coarse-grained potential models for phenyl-based molecules: II. Application to fullerenes. J Phys Chem B 114:6394–6400
99. Bereau T, Deserno M (2009) Generic coarse-grained model for protein folding and aggregation. J Chem Phys 130:235106
100. Liwo A, Pincus MR, Wawak RJ, Rackovsky S, Scheraga HA (1993) Prediction of protein conformation on the basis of a search for compact structures—test on avian pancreatic-polypeptide. Protein Sci 2:1715–1731
101. Maisuradze GG, Senet P, Czaplewski C, Liwo A, Scheraga HA (2010) Investigation of protein folding by coarse-grained molecular dynamics with the UNRES force field. J Phys Chem A 114:4471–4485
102. Ha-Duong T (2010) Protein backbone dynamics simulations using coarse-grained bonded potentials and simplified hydrogen bonds. J Chem Theory Comput 6:761–773
103. Alemani D, Collu F, Cascella M, Dal Peraro M (2010) A nonradial coarse-grained potential for proteins produces naturally stable secondary structure elements. J Chem Theory Comput 6:315–324
104. Ayton GS, Noid WG, Voth GA (2007) Multiscale modeling of biomolecular systems: in serial and in parallel. Curr Opin Struc Biol 17:192–198
105. Peter C, Kremer K (2009) Multiscale simulation of soft matter systems—from the atomistic to the coarse-grained level and back. Soft Matter 5:4357–4366
106. Rzepiela AJ, Schafer LV, Goga N, Risselada HJ, De Vries AH, Marrink SJ (2010) Software news and update reconstruction of atomistic details from coarse-grained structures. J Comput Chem 31:1333–1343
107. Rzepiela AJ, Sengupta D, Goga N, Marrink SJ (2010) Membrane poration by antimicrobial peptides combining atomistic and coarse-grained descriptions. Faraday Discuss 144:431–443
108. Neri M, Anselmi C, Cascella M, Maritan A, Carloni P (2005) Coarse-grained model of proteins incorporating atomistic detail of the active site. Phys Rev Lett 95:218102
109. Nielsen SO, Bulo RE, Moore PB, Ensing B (2010) Recent progress in adaptive multiscale molecular dynamics simulations of soft matter. Phys Chem Chem Phys 12:12401–12414
110. Rzepiela AJ, Louhivuori M, Peter C, Marrink SJ (2011) Hybrid simulations: combining atomistic and coarse-grained force fields using virtual sites. Phys Chem Chem Phys 13:10437–10448
111. Zoete V, Grosdidier A, Michielin O (2009) Docking, virtual high throughput screening and in silico fragment-based drug design. J Cell Mol Med 13:238–248
112. Andrusier N, Mashiach E, Nussinov R, Wolfson HJ (2008) Principles of flexible protein-protein docking. Proteins 73:271–289